



AFRL-RY-HS-TR-2010-0016

---

New Shape Parameters for the Laminar, Transitional, and Turbulent Velocity Profiles

David W. Weyburne

AFRL/RYHC  
80 Scott Drive  
Hanscom AFB, MA 01731-2909

15 December 2008

In-House Technical Report

APPROVED FOR PUBLIC RELEASE; DISTRIBUTION UNLIMITED
---


AIR FORCE RESEARCH LABORATORY  
Sensors Directorate  
Electromagnetics Technology Division  
Hanscom AFB MA 01731-2909


## NOTICE AND SIGNATURE PAGE

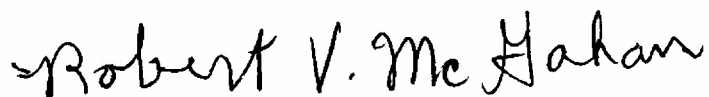
Using Government drawings, specifications, or other data included in this document for any purpose other than Government procurement does not in any way obligate the U.S. Government. The fact that the Government formulated or supplied the drawings, specifications, or other data does not license the holder or any other person or corporation; or convey any rights or permission to manufacture, use, or sell any patented invention that may relate to them.

This report was cleared for public release by the Electronic Systems Center Public Affairs Office for the Air Force Research Laboratory Electromagnetic Technology Division and is available to the general public, including foreign nationals. Copies may be obtained from the Defense Technical Information Center (DTIC) (<http://www.dtic.mil>).

AFRL-RY-HS-TR-2010-0016 HAS BEEN REVIEWED AND IS APPROVED FOR PUBLICATION IN ACCORDANCE WITH ASSIGNED DISTRIBUTION STATEMENT.

  
DAVID WEYBURN  
Contract Monitor

  
DAVID F. BLISS, Acting Chief  
Optoelectronic Technology Branch

  
DR. ROBERT V. MCGAHAN  
Technical Communications Advisor  
Electromagnetics Technology Division

This report is published in the interest of scientific and technical information exchange, and its publication does not constitute the Government's approval or disapproval of its ideas or findings.

REPORT DOCUMENTATION PAGE			Form Approved OMB No. 0704-0188		
Public reporting burden for this collection of information is estimated to average 1 hour per response, including the time for reviewing instructions, searching existing data sources, gathering and maintaining the data needed, and completing and reviewing this collection of information. Send comments regarding this burden estimate or any other aspect of this collection of information, including suggestions for reducing this burden to Department of Defense, Washington Headquarters Services, Directorate for Information Operations and Reports (0704-0188), 1215 Jefferson Davis Highway, Suite 1204, Arlington, VA 22202-4302. Respondents should be aware that notwithstanding any other provision of law, no person shall be subject to any penalty for failing to comply with a collection of information if it does not display a currently valid OMB control number. <b>PLEASE DO NOT RETURN YOUR FORM TO THE ABOVE ADDRESS.</b>					
1. REPORT DATE (DD-MM-YYYY) 15-12-2008		2. REPORT TYPE Technical Report		3. DATES COVERED (From - To) 1 Dec 2006 – 1 Dec 2008	
4. TITLE AND SUBTITLE  New Shape Parameters for the Laminar, Transitional, and Turbulent Velocity Profiles			5a. CONTRACT NUMBER In-House		
			5b. GRANT NUMBER		
			5c. PROGRAM ELEMENT NUMBER 624916		
6. AUTHOR(S)  David W. Weyburne			5d. PROJECT NUMBER 4916		
			5e. TASK NUMBER HC		
			5f. WORK UNIT NUMBER 01		
7. PERFORMING ORGANIZATION NAME(S) AND ADDRESS(ES)  AFRL/RYHC 80 Scott Drive Hanscom AFB, MA 01731-2909			8. PERFORMING ORGANIZATION REPORT NUMBER		
9. SPONSORING / MONITORING AGENCY NAME(S) AND ADDRESS(ES) Electromagnetics Technology Division Sensors Directorate Air Force Research Laboratory 80 Scott Drive Hanscom AFB, MA 01731-2909 Source Code: 437890			10. SPONSOR/MONITOR'S ACRONYM(S) AFRL/RYHC		
			11. SPONSOR/MONITOR'S REPORT NUMBER(S) AFRL-RY-HS-TR-2010-0016		
12. DISTRIBUTION / AVAILABILITY STATEMENT  DISTRIBUTION A: APPROVED FOR PUBLIC RELEASE: DISTRIBUTION UNLIMITED					
13. SUPPLEMENTARY NOTES The U.S. Government is joint author of this work and has the right to use, modify, reproduce, release, perform, display, or disclose the work. Cleared for Public Release by 66 ABW-2010-0138, 8 February 2010.					
14. ABSTRACT In this report a new method for describing the shape and thickness of 2-D wall bounded boundary layer velocity profiles is presented. The new method is based on calculating parameters using simple integrals of the velocity profile. It is shown that these new parameters can be used to describe both the inner and outer region of the turbulent boundary layer, as well as laminar and transitional velocity profiles. Applied to experimental laminar-turbulent profiles, it is shown that one of the new shape parameters foretells the beginning of the laminar-turbulent transition on a flat plate at a much lower Reynolds number than the traditional $H_{12}$ criteria. Furthermore, using another new parameter it is shown that the transition to fully turbulent flow may proceed as a discontinuous event.					
15. SUBJECT TERMS  Fluid Boundary Layers, Velocity Profiles, Turbulent Flow, Laminar Flow, Transition Flow					
16. SECURITY CLASSIFICATION OF:			17. LIMITATION OF ABSTRACT  SAR	18. NUMBER OF PAGES  24	19a. NAME OF RESPONSIBLE PERSON David W. Weyburne
a. REPORT Unclassified	b. ABSTRACT Unclassified	c. THIS PAGE Unclassified			19b. TELEPHONE NUMBER n/a



## Contents

List of Figures .....	iv
List of Tables .....	v
Acknowledgments .....	vi
Summary .....	1
1. Introduction .....	2
2. Moment Description of the Boundary Layer .....	3
2.1 Viscous Velocity Moments .....	3
2.2 Velocity Derivative Moments .....	4
2.3 Velocity Profile Moments .....	5
3. Experimental Application .....	5
3.1 Laminar Flow .....	5
3.2 Experimental Laminar-Turbulent Transitional Flow .....	6
3.3 Turbulent Flow .....	9
3.4 Numerical Calculation of Parameters .....	10
4. Discussion .....	11
5. Conclusion .....	13
References .....	14

## List of Figures

Figure 1. Shape factor, $H_{12}$ , for the T3A ( $\times$ ), T3Am (+), and T3B (*) datasets. ....	7
Figure 2. $\mu_1$ for the T3A ( $\times$ ), T3Am (+), and T3B (*) datasets. ....	7
Figure 3. The normalized T3A velocity profiles. ....	8
Figure 4. The first derivative skewness for the T3A ( $\times$ ), T3Am (+), and T3B (*) datasets. ....	8
Figure 5. T3Am velocity profiles plotted using the Blasius scalings for $Re_x=1.23\times 10^5$ to $1.04\times 10^6$ . ....	9
Figure 6. Numerically calculated second derivatives of Österlund's SW981129 data set. ....	9
Figure 7. $\delta_1 / \mu_1$ for T3B (*), SW981129 ( $\times$ ), SW981005 (+), and SW981113 ( $\circ$ ) datasets. ....	10
Figure 8. $\delta_1 / \mu_1$ for T3B (*), T3A ( $\times$ ), and T3Am (+) datasets. ....	11

## List of Tables

Table 1. Laminar Flow Boundary Layer Parameters .....	6
---	---

## **Acknowledgement**

The author would like to acknowledge the support of the Electromagnetics Technology Division of the Sensors Directorate of the Air Force Research Laboratory. In addition, the author would like to thank Jens Österlund and P. Roach and D. Brierly for supplying their experimental datasets for inclusion in this manuscript.



**Summary** In this report a new method for describing the shape and thickness of 2-D wall bounded boundary layer velocity profiles is presented. The new method is based on calculating parameters using simple integrals of the velocity profile. It is shown that these new parameters can be used to describe both the inner and outer region of the turbulent boundary layer, as well as laminar and transitional velocity profiles. Applied to experimental laminar-turbulent profiles, it is shown that one of the new shape parameters foretells the beginning of the laminar-turbulent transition on a flat plate at a much lower Reynolds number than the traditional  $H_{12}$  criteria. Furthermore, using another new parameter it is shown that the transition to fully turbulent flow may proceed as a discontinuous event.

## 1. Introduction

Prandtl [1] introduced the concept of a boundary layer for fluid flow past a solid over a hundred years ago. Despite tremendous advances in the field, the mathematical tools for describing the thickness and the shape of the velocity or temperature profiles of 2-D wall bounded flows have remained rather limited. A consequence of this lack of descriptive tools is that it is not possible to easily differentiate *mathematically* between laminar, transitional, and turbulent velocity profiles. Currently the most common method is to calculate the shape parameter  $H_{12}$ , which is the ratio of the displacement thickness and the momentum thickness. For  $H_{12} > 2.59$  the profile is considered laminar, for  $H_{12} < 1.4$  the profile is considered turbulent, and for values of  $H_{12}$  in between, the profile is considered transitional [2].

There is no doubt that the  $H_{12}$  parameter has been useful for describing the shape and detecting transition. However, one has to wonder whether there is some other mathematical feature of the boundary layer velocity profile that could help identify and quantify transition behavior. Most practitioners in the field can tell by a simple glance at a profile plot whether it is laminar or turbulent. What property of the boundary layer profile makes this possible? The shape parameter  $H_{12}$  works but it is not obvious why it works. The question is, are there other, possibly better, descriptive tools of the velocity profile. We believe this is in fact the case, as we show below. In what follows, a new method of describing the thickness and shape of 2D wall bounded velocity profiles is outlined. The new tools are useful for describing laminar, turbulent, and laminar-turbulent transition velocity boundary layer profiles. Using one of these parameters, we show that it is possible to detect the onset of laminar-turbulent transition at a much lower Reynolds number than the traditional  $H_{12}$  method. Furthermore, another new parameter is able to show the turbulent transition point as a sharply defined discontinuity when plotted versus plate distance.

The new boundary layer description is an extension of an earlier work in which a mathematically unique way of defining the boundary layer thickness and shape for laminar flow was presented [3]. The method was based on the observation that, for laminar flow over a flat plate, the second derivative of the stream-wise velocity (or temperature) in the direction normal to the plate has a Gaussian-like profile. Borrowing from probability density function methodology, the boundary layer was then described in terms of the central moments of this Gaussian-like kernel. The most important results of this approach are: 1) a mathematically well-defined measure of the laminar boundary layer thickness and 2) four additional parameters that help describe the shape of the laminar boundary layer profile. These four parameters are the mean location, the boundary layer width, the velocity profile skewness, and the velocity profile excess. In the present report, this same second derivative based moment method is shown to track the so-called “inner viscous region” of the turbulent boundary layer.

The question arose as to whether there are other integral kernels that could track the outer region of the transitional and turbulent boundary layers rather than just the inner region. From an experimental standpoint, the stream-wise velocity  $u(y)$  measured at many points normal to the plate ( $y$ -direction) is the only easily accessible velocity quantity of the boundary layer for flow along a plate or wedge ( $x$ -direction). We therefore looked at a number of possible integral kernels involving the stream-wise velocity profile and/or its derivatives. Various possibilities were tested including  $1 - u(y)/u_e$  (where  $u_e$  is the free stream velocity at the

boundary layer edge) and the first derivative of the stream-wise velocity in the direction normal to the plate. Both of these integral kernels can be shown to track the behavior of the outer region of the turbulent boundary layer. It must be emphasized that all of these new moment-based parameters are calculated as simple integrals of the experimental profile data.

To demonstrate the utility of the new descriptive tools, experimental data for the laminar-turbulent transition on a flat plate with a zero-pressure gradient are examined. The experimental data sets are part of the ERCOFLAC test data generated at the Rolls-Royce Applied Science Laboratory, Derby, U.K. and are available on the Internet. The data sets examined include the T3A, T3Am, and T3B cases for laminar-turbulent boundary layer transition [4]. In order to provide baseline data, we also examine purely laminar and purely turbulent data sets. For the laminar flow case, we use the theoretical Blasius [5] solution for laminar flow on a flat plate. For the turbulent flow case, we use the flat plate data from Osterlund [6]. We begin by first reviewing the viscous boundary layer description and then introduce two new boundary layer descriptions.

## 2. Moment Description of the Boundary Layer

### 2.1 Viscous Velocity Moments

In a recent paper Weyburne [3] introduced a boundary layer thickness description based on the second derivatives of the stream-wise velocity  $u(y)$  in the direction normal to the plate ( $y$ -direction). Since the second derivative of the velocity is related to the viscous term in the momentum balance equation, we have termed this the “viscous” boundary layer description. To put the new formulation in the proper perspective, we first briefly review the relevant equations for this viscous boundary layer description.

The mathematical description of the viscous boundary layer region borrows from probability density function (PDF) methodology and is based on central moments of the second derivative-based kernel. For wall-bounded 2-D flow over a wedge, we define the viscous velocity boundary layer  $n$ th central moment,  $\lambda_n$  as

$$\lambda_n \equiv \int_0^h dy (y - \mu_1)^n \frac{d^2 \{-\mu_1 u(y)/u_e\}}{dy^2}, \quad (1)$$

where  $y=h$  is deep into the free stream,  $u_e$  is the free stream velocity at the boundary layer edge, and where the first moment about the origin,  $\mu_1$ , is the normalizing parameter obtained as the requirement that the zeroth moment have a value of unity. The derivative in Eq. 1 is written in this way to emphasize the probability-density-function-like behavior. To completely encompass all flows between laminar and turbulent, we emphasize that the velocity  $u(y)$  used herein is the time-averaged mean value of the stream-wise velocity.

Borrowing from probability density function language, the first moment about the origin,  $\mu_1$  is called the “mean” location of the viscous boundary layer. The mean location of the viscous boundary layer  $\mu_1$  can be shown to be given by

$$\frac{u_e}{\mu_1} = \frac{du(y)}{dy} \Big|_{y=0}, \quad (2)$$

which means it is related to the wall shear stress  $\tau_w$  by  $\mu_1 = \rho \nu u_e / \tau_w$  where  $\nu$  is the kinematic viscosity and  $\rho$  is the density. The second central moment is related to a parameter we call the viscous boundary layer width given by  $\sigma_v = \sqrt{\lambda_2}$ . The physical description of the shape of the viscous boundary layer is extended by using the third and fourth moments to define the viscous boundary layer skewness  $\gamma_{1v} = \lambda_3 / \sigma_v^3$  and the viscous boundary layer excess  $\gamma_{2v} = \lambda_4 / \sigma_v^4 - 3$ .

Borrowing from probability density function methodology, the definition of the viscous boundary layer thickness  $\delta_v$ , defined as the point at which the viscous contributions to the stream-wise velocity component becomes negligible, is taken as  $\delta_v = \mu_1 + 2\sigma_v$ . It should be noted that the probability community sometimes uses the mean plus three times  $\sigma$  (or even six times  $\sigma$  as in “six sigma”) instead of two sigma as used herein. Any of the definitions can be used as long as it is clear which of the definitions is being used. The two sigma value was chosen so that  $\delta_v$  approximately tracks the 99% thickness  $\delta_{99}$  for laminar flow.

In order to calculate the moments in Eq. 1 without having to differentiate the experimental data, a process known to cause problems when noise is present, we introduce a set of auxiliary integrals given by

$$\alpha_n \equiv \int_0^h dy y^n (1 - u(y)/u_e) \quad (3)$$

By integrating by parts, it is a simple matter to show that the viscous moments are given by  $\lambda_2 = -\mu_1^2 + 2\mu_1\alpha_0$ ,  $\lambda_3 = 2\mu_1^3 - 6\mu_1^2\alpha_0 + 6\mu_1\alpha_1$ , and  $\lambda_4 = -3\mu_1^4 + 12\mu_1^3\alpha_0 - 24\mu_1^2\alpha_1 + 12\mu_1\alpha_2$ , respectively. Note that  $\alpha_0$  is equal to the displacement thickness  $\delta_1$ .

## 2.2 Velocity Derivative Moments

In addition to the second derivative kernel, we investigated other integral kernels for describing the boundary layer. After looking at various possibilities, we found that the kernel based on the derivative of the stream-wise flow velocity in the direction normal to the plate has the right PDF-like characteristics. We therefore define the derivative of the stream-wise velocity boundary layer  $n$ th moment,  $\kappa_n$  as

$$\kappa_n \equiv \int_0^h dy (y - \delta_1)^n \frac{d\{u(y)/u_e\}}{dy}, \quad (4)$$

such that  $\kappa_0$  is normalized to one,  $y = h$  is deep into the free stream, and the mean location of the derivative of the stream-wise velocity profile is the displacement thickness  $\delta_1$  given by

$$\delta_1 \equiv \int_0^h dy \{1 - u(y)/u_e\} \quad (5)$$

The stream-wise velocity boundary layer width is defined as  $\sigma_s = \sqrt{\kappa_2}$ . To calculate these moments without having to calculate the derivative, we can integrate by parts and use the set of auxiliary integrals  $\alpha_n$  given by Eq. 3. This means that stream-wise velocity boundary layer width, for example, can be calculated without differentiating the data, as  $\sigma_s^2 = -\delta_1^2 + 2\alpha_1$ . Just as in the viscous boundary layer description, we extend the physical description of the velocity derivative boundary layer by using the third and fourth moments to define the velocity derivative boundary layer skewness  $\gamma_{1s} = \kappa_3 / \sigma_s^3$  and the velocity derivative boundary layer excess  $\gamma_{2s} = \kappa_4 / \sigma_s^4 - 3$ . Integrating by parts and using  $\alpha_n$ , it is easy to show that the third and fourth moments are  $\kappa_3 = 2\delta_1^3 - 6\delta_1\alpha_1 + 3\alpha_2$  and  $\kappa_4 = -3\delta_1^4 + 12\delta_1^2\alpha_1 - 12\delta_1\alpha_2 + 4\alpha_3$ .

The definition of the stream-wise boundary layer thickness  $\delta_s$  is defined as the point at which the stream-wise velocity derivative components become negligible. To approximately track the 99% thickness  $\delta_{99}$  for turbulent flow, the thickness is taken as  $\delta_s = \delta_1 + 3\sigma_s$ .

### 2.3 Velocity Profile Moments

In addition to the derivative kernels, we posit that the velocity boundary layer may also be described in terms of moments of  $1 - u(y)/u_e$ . Thus, we define the velocity boundary layer  $n$ th moment  $\zeta_n$  as

$$\zeta_n \equiv \int_0^h dy (y - m)^n \frac{1}{\delta_1} \{1 - u(y)/u_e\} \quad , \quad (6)$$

such that  $\zeta_0$  is normalized to one,  $y = h$  is deep into the free stream, and where the mean location of the stream-wise velocity profile is given by

$$m \equiv \int_0^h dy y \frac{1}{\delta_1} \{1 - u(y)/u_e\} \quad . \quad (7)$$

The velocity boundary layer width is defined as  $\sigma_u = \sqrt{\zeta_2}$ . It is straightforward to calculate the skewness and excess using the first four moments. The boundary layer thickness  $\delta_u$  will be defined as  $\delta_u = m + 3\sigma_u$ . Notice that these velocity profile moments are closely related to the set of auxiliary integrals given by  $\alpha_n$  (Eq. 3). This means that all three of the moment-based descriptions can be calculated using the auxiliary integrals  $\alpha_n$  (Eq. 3).

## 3. EXPERIMENTAL APPLICATION

### 3.1 Laminar Flow

Before we look at the laminar-turbulent transition, it is necessary to provide a laminar flow baseline description. For the laminar flow case we will use the Blasius [5] boundary layer

solution to the flow-governing equations that is known to describe experimental laminar flow profiles very well [2]. It is easily verified for the Blasius flow that  $\delta_1 = 1.7209\sqrt{\nu x/u_e}$  and that the stream-wise boundary layer width on the flat plate is given by  $\sigma_s = 1.1852\sqrt{\nu x/u_e}$ . This means that the stream-wise boundary layer thickness is given by  $\delta_s = 5.3\sqrt{\nu x/u_e}$ . The physical description of the “stream-wise” velocity boundary layer is extended by using the third and fourth moments to define the stream-wise velocity derivative boundary layer skewness,  $\gamma_{1s} = \kappa_3/\sigma_s^3$  and the stream-wise velocity boundary layer excess  $\gamma_{2s} = \kappa_4/\sigma_s^4 - 3$ . For the Blasius flow case, the third moment is given by  $\kappa_3 = 1.1647(\nu x/u_e)^{3/2}$  which means that  $\gamma_{1s} = 0.70$ . Finally, the fourth moment is given by  $\kappa_4 = 6.0(\nu x/u_e)^2$  which means that  $\gamma_{2s} = 0.041$ . Note that if the velocity derivative profile was purely Gaussian then  $\gamma_{1s} = \gamma_{2s} = 0$ .

The results for all three moment method descriptions of the Blasius solution are summarized in Table 1. Laminar-like flow is indicated when the **ratio** of the velocity or first derivative moment thickness parameters to the viscous second derivative boundary layer thickness parameter values is similar to the values calculated from Table 1.

**Table 1: Laminar Flow Boundary Layer Parameters**

Kernel	Mean Location	Width	Skewness	Excess
Second Deriv.	$\mu_1 = 3.0115\sqrt{\nu x/u_e}$	$\sigma_v = 1.138\sqrt{\nu x/u_e}$	$\gamma_{1v} = 0.29$	$\gamma_{2v} = -0.08$
First Deriv.	$\delta_1 = 1.7209\sqrt{\nu x/u_e}$	$\sigma_s = 1.185\sqrt{\nu x/u_e}$	$\gamma_{1s} = 0.70$	$\gamma_{2s} = 0.04$
Velocity	$m = 1.2685\sqrt{\nu x/u_e}$	$\sigma_u = 1.004\sqrt{\nu x/u_e}$	$\gamma_{1u} = 1.046$	$\gamma_{2u} = 0.041$

### 3.2 Experimental Laminar-Turbulent Transitional Flow

The ERCOFLAC experimental data considered herein consists of a series of velocity profiles taken at various distances along a flat plate with a zero pressure gradient [4]. The intent of these test cases was to investigate the effect of free-stream turbulence on the transition from laminar to turbulent flow on a flat plate. There is considerable interest in being able to identify the point of transition from laminar to turbulent flow. The one traditional method for detecting the onset of laminar-turbulent transition is based on the shape factor  $H_{12}$ , which is calculated and then plotted versus the reduced plate distance,  $Re_x = xu_e/\nu$ . The results for the three ERCOFLAC test cases are presented in Fig. 1. The upper dashed line in the figure is the  $H_{12} = 2.59$  line for laminar flow and the lower dashed line is the  $H_{12} = 1.4$  line for turbulent flow [2]. The start of transition is identified as the point where the plotted lines cross the dashed lines. As expected, the data indicates that as the free-stream turbulence intensity increases from 1% (+) to 3% (x) to 6% (\*), the transition occurs at lower and lower Reynolds number.

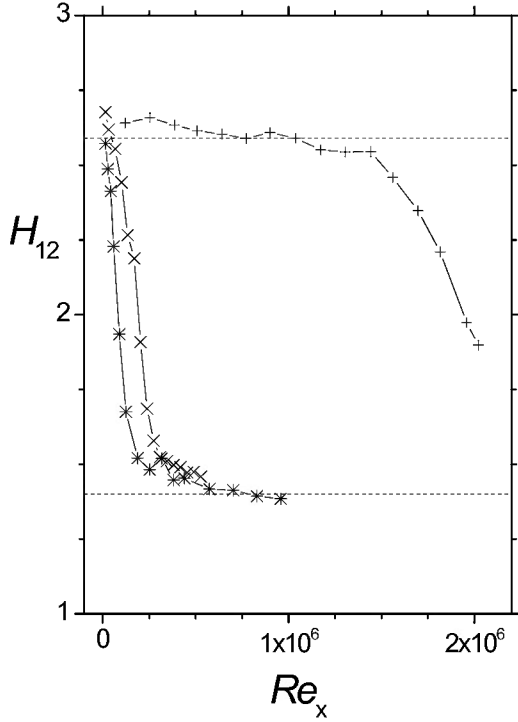


Fig. 1: Shape factor,  $H_{12}$ , for the T3A ( $\times$ ), T3Am ( $+$ ), and T3B ( $*$ ) datasets.

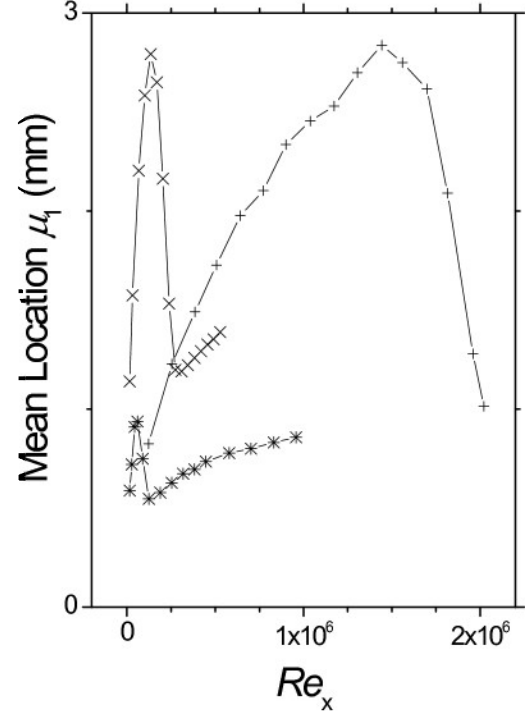


Fig. 2:  $\mu_1$  for the T3A ( $\times$ ), T3Am ( $+$ ), and T3B ( $*$ ) datasets.

Now consider the thickness parameter  $\mu_1$  plotted in Fig. 2 versus the Reynolds number for the three test cases. The plots show three distinct behaviors. At the low  $Re_x$  side of each plot, all three start with laminar-like behavior as evidenced by  $H_{12}$  (Fig. 1) or plots of  $\delta_1/\mu_1$  (not shown but which show ratios close to those given by Table 1). As the  $Re_x$  initially increases, the  $\mu_1$  values increase until they peak. These  $\mu_1$  values are laminar-like and have values close to those calculated from Table 1. After the peak, the  $\mu_1$  values begin to decline. We attribute this behavior to transition profile behavior. Finally, there is an abrupt change in the slope and the value of  $\mu_1$  begins to increase again (except the T3Am case which Fig. 1 also indicates does not reach the fully turbulent line). We believe the  $Re_x$  at the point of the slope discontinuity is the turbulent transition point and the profiles on the increasing  $\mu_1$  side of the discontinuity are fully turbulent profiles. In order to see this behavior better, we plot the sixteen velocity profiles for the T3A case in Fig. 3. The laminar-like and turbulent-like profiles are labeled and color-coded black. The one blue line profile corresponds to the peak  $\mu_1$  value in Fig. 2. The red lines in Fig. 3 correspond to the transitional profiles characterized by decreasing  $\mu_1$  values. The correlation to the behavior of the  $\mu_1$  parameter is easily observable.

Thus far we have only considered the mean location  $\mu_1$ . After examining a number of other parameter plots and ratio plots, we found some very interesting behavior of the first derivative skewness  $\gamma_{1s}$  (Section 2.2), shown plotted in Fig. 4. The dashed line represents the laminar flow

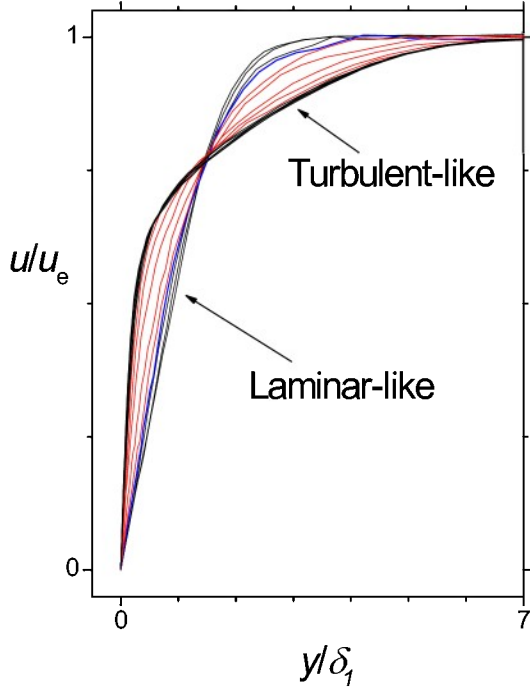


Fig. 3: The normalized T3A velocity profiles.

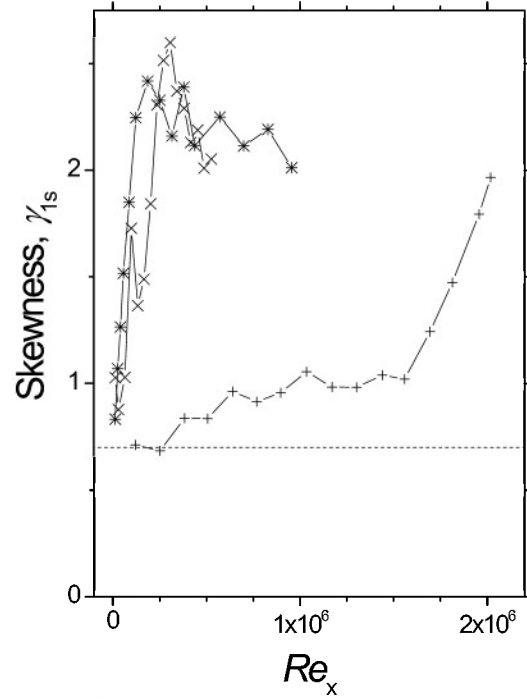


Fig. 4: The skewness  $\gamma_{1s}$  for the T3A ( $\times$ ), T3Am (+), and T3B (\*) datasets.

limit (Table 1). The plot indicates that for the T3Am (+) case, the flow profiles start to become more skewed and begin to differ from the laminar flow-like behavior at  $Re_x \sim 0.25 \times 10^6$ . This is significantly earlier than the thickness-based criteria  $H_{12}$  (Fig. 1). This is not to say that transition occurs at this  $Re_x$  but rather this is the point where we first observe the signs of an impending transition. Plots of the first derivative excess  $\gamma_{2s}$  (not shown) also show similar behavior to the stream-wise skewness.

In order to better understand what, exactly, these new shape parameters are seeing, it is instructive to look at the T3Am data more closely. In Fig. 5, the first eight stream-wise velocity profiles are plotted versus the reduced normal distance  $y/\sqrt{\nu x/u_e}$  corresponding to  $Re_x$  ranging from  $1.23 \times 10^5$  (1W00908 dataset) to  $1.04 \times 10^6$  (1W01005 dataset). These data profiles were chosen because, based on their  $H_{12}$  values (Fig. 1), they would traditionally all be categorized as laminar flow profiles. For laminar flow, the velocity profiles should all collapse to a single profile using the Blasius scalings. This is obviously not the case as shown in Fig. 5. It is clear from Fig. 5 that the profile behavior close to the wall is changing in a systematic way according to the  $Re_x$ . The profile shape near the wall is changing but there is almost no change in the shape in the outer region, indicating that the profile shape is becoming skewed, just as is indicated by  $\gamma_{1s}$  in Fig. 4. Thus, the new shape parameters  $\gamma_{1s}$  and  $\gamma_{2s}$  are capturing boundary layer profile information that the traditional parameters were not.



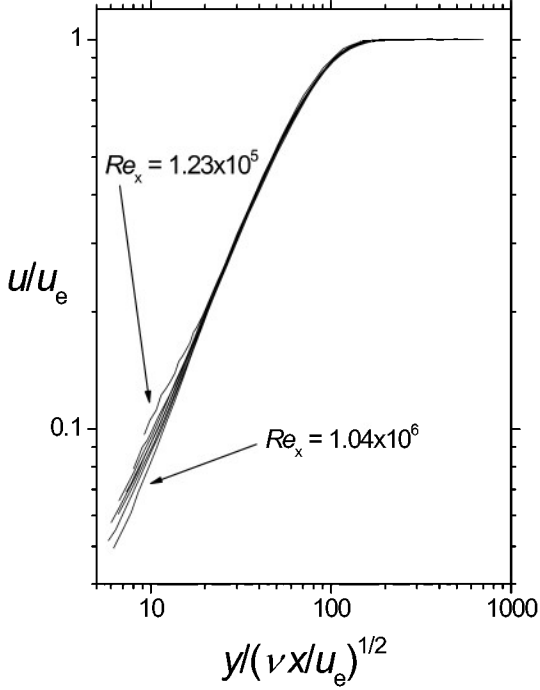


Fig. 5: T3Am velocity profiles plotted using the Blasius scalings.

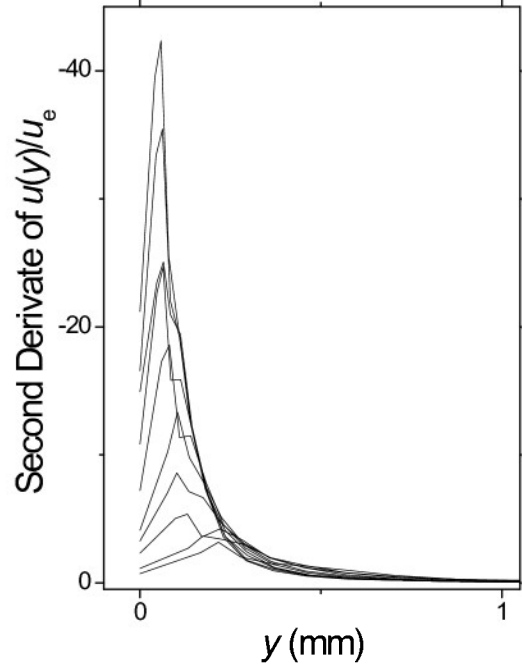


Fig. 6: Numerically calculated second derivatives of Österlund's SW981129 data set.

### 3.3 Turbulent Flow

For the turbulent boundary layer, the determination of the skin friction coefficient  $c_f$  is of much interest. The skin friction coefficient, or equivalently the wall shear stress  $\tau_w$ , is difficult to measure experimentally. From velocity profile data, the Clauser chart method can be used to calculate  $c_f$ , but it is an indirect method requiring certain assumptions. The viscous thickness  $\mu_1$  offers a new way of calculating  $c_f$  and  $\tau_w$  from velocity profile data. The thickness  $\mu_1$  can be calculated by twice numerically differentiating profile data, then integrating the result, and noting  $\lambda_0 = 1$  (Eq. 1). Once  $\mu_1$  is calculated,  $c_f$  and  $\tau_w$  can be calculated using Eq. 2. We have tested this method on a number of high quality, low noise datasets. For example, we found that  $\mu_1$  calculated from Österlund's [6] SW981129 (10 profiles total) profile data deviated by no more than  $\pm 3\%$  from the  $\mu_1$  calculated using Österlund's reported oil-interferometry-based  $c_f$  data. In Fig. 6 we show the calculated second derivative profile data for this data set. Numerical differentiation is known to be problematic in the presence of noise so that the technique will only be usable for data taken with modern technology such as used to gather Österlund's data sets.

The laminar-turbulent flow data indicates that the new shape and thickness parameters have a lower limit consistent with the laminar flow predicted from the Blasius theoretical profile. The question is whether there is an upper limit for the parameters for fully turbulent flow, *i.e.* does

$\delta_1 / \mu_1$ , for example, tend to some numerical constant as the Reynolds number increases. The ratio  $\delta_1 / \mu_1$  is interesting because it tracks the outer layer thickness to the viscous inner layer thickness. As a first attempt to answer this question, we examine the purely turbulent experimental data from Österlund [6] along with the T3B test case, which has some transitional and turbulent profiles (Fig. 1). In Fig. 7 we plot the mean thickness ratio,  $\delta_1 / \mu_1$  for the T3B

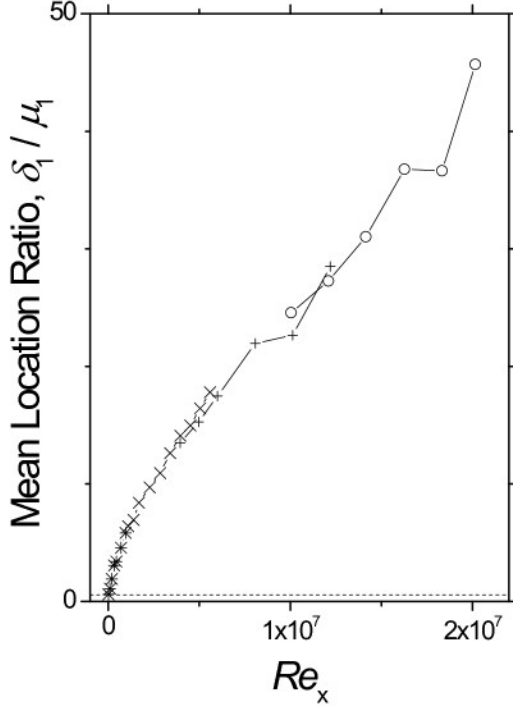


Fig. 7:  $\delta_1 / \mu_1$  for T3B (\*), SW981129 (×), SW981005 (+), and SW981113 (○) datasets.

problem, we rounded all the normalized velocities that were nominally in the free stream to one. The free stream starting point was taken as the first point at which the velocity ratio was greater than or equal to one.

For the numerical calculation of the integrals reported herein, the Trapezoidal Rule was used and the data point,  $u(0) = 0$ , was added to every data set. For all of the moment values except the viscous mean location  $\mu_1$ , the various new parameters were calculated without numerical differentiation using the auxiliary integrals  $\alpha_n$ . In fact, all of the above parameters can be calculated with only four integrals of the velocity profile;  $\alpha_0$ ,  $\alpha_1$ ,  $\alpha_2$ , and  $\alpha_3$  (Eq. 3). For the older datasets, the parameter  $\mu_1$  was calculated from the reported experimental values of the skin friction coefficient. For certain newer datasets, like Österlund's datasets, the integral-moment-calculated  $\mu_1$  values were in good agreement with the values calculated using the reported skin friction coefficient data.

transition case (\*) and three of Österlund's turbulent data sets, SW981129 (×), SW981005 (+), and SW981113 (○) test cases. The test cases were chosen to span Österlund's full  $Re_x$  range. The lower dashed line at  $\delta_1 / \mu_1 \sim 0.57$  corresponds to the laminar flow limit (see Table 1). This plot indicates that there does not appear to be an upper limit for the thickness ratio,  $\delta_1 / \mu_1$ . Likewise, plots of the stream-wise  $\sigma_s / \sigma_v$ , the skewness,  $\gamma_{1s}$ , and the stream-wise excess,  $\gamma_{2s}$  (not shown) do not show an upper limit. Thus, in all cases there does not appear to be an upper limit to any of the new parameters for turbulent boundary layers.

### 3.4 Numerical Calculation of Parameters

The free stream velocity was used in all cases as the normalizing constant for the stream-wise velocity. It was found that in so doing, the normalized values outside the boundary layer region (*i.e.* nominally in the free stream) fluctuated a few thousands about one. This fluctuation caused nontrivial contributions to the calculated higher-order moments. To avoid this

#### 4. Discussion

This new boundary layer moment method is taken directly from the standard mathematical method for describing probability density functions and is already the standard method for describing the temporal behavior of the turbulent flow velocities. Herein, we propose that the probability density function methodology be used to describe the spatial behavior of the velocity profiles as well. The most important result of this approach is that for the first time, we have a mathematically well-defined way to describe the boundary layer thickness and shape. Recall that Schlichting [2] states that “It is impossible to indicate a boundary-layer thickness in an unambiguous way, because the influence of viscosity in the boundary layer decreases asymptotically outwards.” The moment-based method apparently lets us do the impossible. Furthermore, the new boundary layer parameters each have a direct physical interpretation as to the thickness and shape of the profile (*e.g.* the mean location, the skewness). It is not clear what the traditional shape parameters such as  $H_{12}$  are actually describing.

Not only are the new parameters mathematically well defined (as opposed to  $\delta_{99}$  for example), but we now have a set of parameters that truly help define the shape of the profile in the skewness and excess. There are no traditional analogs of these parameters. The traditional  $H_{12}$  and related “shape” parameters are not shape parameters in any normal mathematical sense. Consider the first derivative skewness  $\gamma_{1s}$  (Section 2.2) shape parameter for example. The skewness  $\gamma_{1s}$  is able to see the early signs of laminar-turbulent transition thereby providing a more accurate method of predicting the onset of the transition than the normal criteria  $H_{12}$  (compare Fig. 1 to Figs. 4 and 5).

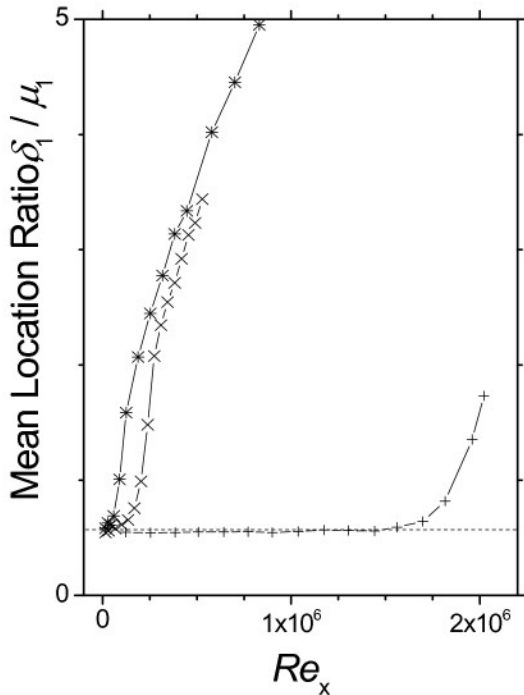


Fig. 8:  $\delta_1 / \mu_1$  for T3B (\*), T3A (x), and T3Am (+) datasets.

The difficulties in understanding turbulent flow behavior have led to the practice of modeling the turbulent profile as two regions, an inner and outer region. The inner region of the turbulent boundary layer is often called the viscous layer since viscosity effects are important in this region. From the flow governing equations, it is self-evident that the viscous effects region will be significant where the second derivative of the velocity is significant. It follows, therefore, that the viscous sublayer can be characterized by moments of the second derivative profile. The new first derivative velocity-profile-based parameters and the velocity-profile-based parameters described herein were introduced to track the outer region of the velocity profile. Thus, for the first time we have a way of simultaneously tracking both the inner and outer regions of the turbulent boundary layer. The ratio of the mean locations should, therefore, provide useful

information as to the behavior of the inner and outer regions of the velocity profile. To verify this, we plot the  $\delta_1/\mu_1$  ratio for the three ERCOFLAC test cases in Fig. 8. The dashed line corresponds to the laminar flow ratio (Table 1). It is readily evident that the ratio starts to differ from the laminar-like flow at the point where transitional velocity profiles begin to appear. Note that the thickness ratios, such as  $H_{12}$  and  $\delta_1/\mu_1$ , are not effective at seeing the early signs of transition as was the case with the skewness  $\gamma_{1s}$ . Taking Figs. 2 and 8 together, we can see that for fully turbulent-like flow, the outer boundary layer is expanding much faster than the inner boundary layer region.

One of the unexpected findings is related to the identity of the displacement thickness  $\delta_1$ . Although this parameter has always been considered useful for calculating  $H_{12}$  for example, it has never been considered a thickness parameter that tracks anything of importance in the boundary layer. However, we now see that  $\delta_1$  is the mean location of the first derivative of the velocity profile (Section 2.2). Therefore, this parameter is actually tracking the outer layer region of the boundary layer. Compare the thickness parameters from Section 2, such as  $\delta_1$  and  $m$ , to the often used 99% thickness  $\delta_{99}$ . The new thickness and shape parameters are all integral quantities whose calculated value involves all of the data points in the data set. The traditional  $\delta_{99}$  thickness, on the other hand, usually involves the use of only a few data points. Furthermore, it is usually necessary to interpolate between the data points to find  $\delta_{99}$ . Since the actual functional form of the transition to the free stream for turbulent flow is unknown, then it is not possible to fit for the  $\delta_{99}$  thickness. Therefore the  $\delta_{99}$  parameter for turbulent experimental datasets is simply ill defined. All one can do is to report a maximum and minimum value that brackets the probable value of  $\delta_{99}$ . The use of the  $\delta_{99}$  parameter has persisted because there have been no good alternatives until now. The new moment-based methods provide a set of mathematically well-defined parameters and will always yield a calculated value (albeit with an associated error bar). Furthermore, all of these new parameters, including the shape parameters, can be calculated from only four simple integrals of the velocity profile,  $\alpha_0$ ,  $\alpha_1$ ,  $\alpha_2$ , and  $\alpha_3$  (Eq. 3).

The new shape parameter  $\mu_1$  shows very interesting behavior. To review, the  $\mu_1$  parameter is the mean location of the second derivative of the velocity profile. If one plotted the second derivative of the velocity, the profiles would be roughly Gaussian-like with the mean location  $\mu_1$  roughly corresponding to the maximum. Therefore, an increase in the value of  $\mu_1$  means that the center of the second derivative profile is shifting away from the wall. It also happens that this parameter is inversely related to the skin friction coefficient (Eq. 2). The well-known behavior of the skin friction coefficient change with Reynolds number during laminar-turbulent transition on a plate [2] is being reflected in the plots of  $\mu_1$  versus the Reynolds number. What is new herein is the realization of what exactly the correlation is between the changes in the skin friction coefficient and the thickness of the viscous sublayer. One of the most distinctive features of the plot of  $\mu_1$  at different stations along the plate (Fig. 3) is the sharp, discontinuous transition to turbulent behavior. It is not the gradual transition one would expect from looking at the  $H_{12}$  plot (Fig. 1). The slopes of the lines before and after transition are noticeably different,

indicating that the transition point may be a singular point. Not surprisingly, this feature is also present in plots of  $c_f$  versus  $Re_x$ . The discontinuity makes it easy to determine the onset of fully turbulent behavior. Consider the T3A case; according to the  $H_{12}$  plot (Fig. 1), none of the T3A ( $\times$ ) profiles are fully turbulent-like. In contrast, Fig. 2 indicates that almost half of the profiles are fully turbulent-like. The failure of the  $H_{12}$  prediction is a reflection of the fact that the transitional  $H_{12}=1.4$  dividing line is based on experimental observations [2] and it should surprise no one familiar with this type of parameterization that the actual dividing line varies from experiment to experiment.

In the earlier paper [3], we considered both the velocity profile and the temperature profile for laminar flow along a flat plate and showed that the temperature flow field can be described in a moment-based manner similar to the velocity flow field. In the present paper, we restricted our attention to the velocity flow case but we want to emphasize that the method is: 1) not restricted to the description of velocity boundary layer but is also applicable to the temperature boundary layer and 2) it is not restricted to flow on a flat plate but should have application to most, if not all, boundary layer flow situations.

## 6. Conclusion

In conclusion, a mathematically unique definition for the boundary layer velocity profile thickness and shape has been extended with a number of additional parameters useful in quantifying the behavior of the velocity profiles of the laminar, turbulent, and transitional boundary layers. The new parameters are able to detect the onset of laminar-turbulent transition at a much lower Reynolds number than the traditional method. Utilizing the new parameters, it was evident that the fully turbulent transition phase may be a singular point transition.

## References

- [1] Prandtl, L., (1904) “Ueber die Flüssigkeitsbewegung bei sehr klner Ribung.” In: Verhandlungen des III. Internationalen Mathematiker-Kongress, Heidelberg, pp. 484–491.
- [2] Schlichting, H., (1979) Boundary Layer Theory. 7th edn., McGraw-Hill, New York.
- [3] Weyburne, D., (2006) “A mathematical description of the fluid boundary layer.” Applied Mathematics and Computation, **175**, pp 1675-1684. Also Weyburne, D., (2008) Erratum to “A mathematical description of the fluid boundary layer”. Applied Mathematics and Computation, **197**, pp 466
- [4] Roach, P., and Brierly, D., (1992) “The Influence of a Turbulent Free-Stream on Zero Pressure Gradient Transitional Boundary Layer Development including the T3A & T3B Test Case Conditions.” In: Pirneau O, Rodi W, Ryming I, Savill A, and Truong T (ed) Numerical Simulation of Unsteady Flows and Transition to Turbulence, Cambridge University Press, New York, pp 319-347
- [5] Blasius, H., (1908), “Grenzschichten in Flüssigkeiten mit kleiner Reibung. Zeitschrift für Mathematik und Physik,” **56**, pp 1-37.
- [6] Österlund, J., (1999) “Experimental studies of zero pressure-gradient turbulent boundary layer.” PhD. Thesis, Dept. of Mechanics, Royal Institute of Technology, Stockholm.